Materials Today Chemistry 28 (2023) 101366

Contents lists available at ScienceDirect

Materials Today Chemistry

journal homepage: www.journals.elsevier.com/materials-today-chemistry/

Enhancement of the intrinsic fluorescence of ZIF-8 via post-synthetic cation exchange with Cd^{2+} and its incorporation into PDMS films for selective sulfide optical sensing

F.G. Moscoso [a], L.M. Rodriguez-Albelo [b], A.R. Ruiz-Salvador [a, **], Tânia Lopes-Costa [a], J.M. Pedrosa [a, *]

[a] Departamento de Sistemas Físicos, Químicos y Naturales, Universidad Pablo de Olavide, Ctra. Utrera Km. 1, Seville, 41013, Spain
[b] Departamento de Ingeniería y Ciencia de Los Materiales y Del Transporte, Universidad de Sevilla, Escuela Politécnica Superior, Calle Virgen de África, 7, Seville, 41011, Andalucía, Spain

ARTICLE INFO

Article history:
Received 19 September 2022
Received in revised form
30 November 2022
Accepted 16 December 2022
Available online xxx

Keywords:
Metal-organic frameworks
Zeolitic imidazolate frameworks
Post-synthetic modification
Photoluminescence
Sensor

ABSTRACT

In this study, ZIF-8 MOF nanocrystals were synthesized and post-synthetically modified by applying different cation exchange strategies. Addition of cadmium nitrate in either methanol or DMF followed by either magnetic stirring or gentle heating led to the incorporation of a small amount of Cd (II) ions into the crystal structure in most cases, as clearly demonstrated by several characterization techniques including PXRD, SEM-EDS and FT-IR. This novel doped material exhibits a high fluorescence with the maximum emission wavelength at 444 nm upon excitation at 380 nm, which allows its use as an effective optical sensor. The sensing capability of the Cd-doped ZIF-8 material was demonstrated by its exposure to sulfide ions in aqueous solution. The fluorescence of the doped material was gradually quenched as the concentration of S^{2-} was increased. Sensing devices based on mixed-matrix membranes (MMMs) were fabricated by using poly (dimethyl siloxane) (PDMS) as a hosting matrix for the Cd-doped ZIF-8 crystals, giving rise to fluorescent sensing films with fast and selective responses against a broad number of potential interferents.

1. Introduction

Metal-Organic Frameworks (MOFs) are a class of hybrid materials assembled by the linkage of metals ions (or clusters) and organic ligands, forming extended two- or three-dimensional crystalline networks with high porosity [1,2]. Based on the large variety of metals and potential organic linkers, MOFs are used in numerous research fields like gas storage [3,4] and separation [5–7], drug delivery [8,9], catalysis [10–15], or chemical sensing [16–22] among others [23–25]. Moreover, the possibility of carrying out post-synthetic modifications (PSMs) of their structures is a way to increase the number of MOFs with tailored properties and thus enhancing the MOFs capabilities in applications like light emission or gas adsorption [26,27]. PSM is especially interesting for sensing applications, where the ligands or/and metal nodes play an essential role in adsorption, reactivity and selectivity [18].

Zeolitic Imidazolate Frameworks (ZIFs) are a sub-class of MOFs where transition metal ions, usually Zn (II) or Co (II), are tetrahedrally-coordinated to the N atoms of imidazolates (Im) [28]. In this class of materials, the angle between two metal centres bridged by an imidazolate unit (M–Im–M) is similar to the Si–O–Si angle found in zeolites. For this reason, ZIFs are typically isoreticular to zeolites, like *sod, rho* or *ana* among others [29]. In particular, ZIF-8 has been widely studied because of its thermal and chemical stability and many synthetic routes have been designed for its preparation. ZIF-8 is formed by the coordination between Zn (II) and 2-methylimidazole (2-me-Im) with *sod* type structure [29,30]. Within the sensing applications, ZIF-8 has been generally used as electrochemical sensor [31–38] and its use as optical sensor limits its role as hosting matrix, requiring the incorporation of emissive cargos like carbon dots [39,40], fluorescent molecules/dyes or lanthanide ions [41–49]. However, to the best of our knowledge, pure ZIF-8 has been rarely employed as optical sensor

* Corresponding author.
** Corresponding author.
E-mail addresses: rruisal@upo.es (A.R. Ruiz-Salvador), jmpedpoy@upo.es (J.M. Pedrosa).

https://doi.org/10.1016/j.mtchem.2022.101366

because it exhibits almost no fluorescence and therefore a very poor sensing response [50], which are the main drawbacks of this material for this specific application.

The high toxicity of the S^{2-} ion poses a significant harm to both the ecological systems (specially aquatic life) and human health. For humans, direct exposure to low concentrations of sulphide ions can cause localized inflammation and irritation in wet membranes, such as eyes and respiratory tract, and even long-term exposure could provoke chronic health disease [51,52]. In addition, high concentrations of the S^{2-} ion result in severe human disorders like pulmonary edema, respiratory or nervous system paralysis and can even be lethal at concentrations above 500 ppm [53]. In this sense, the concentration of S^{2-} ions has been an important index in biological, environmental, and health systems. Therefore, simple, fast, and selective detection of S^{2-} ion is highly necessary.

In this context, nanosized ZIF-8 particles were synthesized, and a post-synthetic cation exchange was successfully carried out doping the original material with a small number of Cd atoms (1–5% of total metal ions), enhancing the intrinsic luminescent properties of the MOF for its subsequent use as an effective optical sensor. For this purpose, the sensing capabilities of the new material have been applied to the detection and quantification of sulfide ions in aqueous media. Additionally, the Cd-doped ZIF-8 crystals were embedded in nanoporous poly(dimethylsiloxane) (PDMS) membranes [54], giving rise to sensing films with high response rates and selectivity towards the target analyte.

It is worth mentioning that previously reported bimetallic Zn/Cd ZIF-8 materials have large particle sizes, non-homogeneous particle size distribution, and in any case their luminescent properties have not been investigated [55,56]. Therefore, the enhancement of the emission capacity of pure ZIF-8 found in this work, just being doped with Cd(II) ions, while maintaining its structural properties almost unaltered, paves the way for the use of this well-known versatile material in those applications where high luminescence is required like optical sensing.

2. Experimental section

2.1. Materials and methods

Zinc (II) nitrate hexahydrated, $Zn(NO_3)_2{\cdot}6H_2O$ (> 99%), 2-methylimidazole, cadmium (II) nitrate hexahydrated, $Cd(NO_3)_2{\cdot}6H_2O$ (> 99%) and sodium sulfide nonahydrated $Na_2S{\cdot}9H_2O$ (≥98%) were all purchased from Sigma-Aldrich. Poly(-dimethylsiloxane) (Synglard® 184) was purchased from Dow Corning. Other reagents and solvents were purchased as reagent grade and used without further purification.

Powder X-ray diffraction (PXRD) analysis was performed on approximately 10–15 mg of each sample at room temperature using a Bruker D8 Discover diffracttometer at 50 kV and 1000 mA for Cu kα ($\lambda = 1.5418$ Å), in the range 5°-50° 2θ with a step of 0.02° per 0.5 s. In addition, X-ray microdiffraction (μ-XRD) was used for the MOF@PDMS membranes. The shape and size of the MOFs particles were examined by scanning electron microscopy (SEM), using a FEI Teneo and by high resolution transmission electron microscopy (HR- TEM), using a FEI Talos F200X. For this purpose, a droplet of an aqueous suspension of particles was deposited onto a copper grid coated with a thin carbon layer and dried in air. The particle size distributions were obtained from the HR-TEM images by counting one hundred particles and analysed by the ImageJ software. Thermogravimetric analysis (TGA) was performed by analyzing approximately 10–15 mg of sample under an air atmosphere using a TGA Discovery apparatus (TA instruments) running from room temperature until 1000 °C with a heat rate of 10 °C/min. For semiquantitative elemental analysis, Scanning electron microscopy-Energy dispersed X-ray spectroscopy (SEM-EDS; FEI Teneo) and Wavelength Dispersive X-ray Fluorescence (WDXRF; Malvern Pananalytical AXIOS equipped with a Rh tube) were used. FT-IR transmittance spectra were recorded with a IFS-66s (Bruker) using a scanner velocity of 2.2 KHz and a resolution of 4 cm^{-1}. For these measurements, the compounds were dispersed in ethanol and a drop of this dispersion was deposited onto a Si substrate that was placed on the sample holder. Fluorescence (FL) emission and excitation spectra were recorded with a Hitachi FL-7000 Fluorescence Spectrophotometer. For FL emission measurements, a high pass filter at 400 nm was used.

2.2. ZIF-8 synthesis

The ZIF-8 synthesis proposed by J. Cravillon et al. [57] was followed with some modifications. Briefly, 448.95 mg (1 eq.) of $Zn(NO_3)_2{\cdot}6H_2O$ was dissolved in 30 cm^3 (350 eq.) of methanol. Parallelly, 973.35 mg (8 eq.) of 2-methylimidazole were also dissolved in another 30 cm^3 of methanol. Then, the 2-methylimidazole solution was rapidly poured into the Zinc (II) solution under magnetic stirring. After 1 h, the reaction was stopped and the white precipitate was separated from the dispersion by centrifugation at 6500 rpm and washed three times with fresh methanol. The crystals were dried in air at room temperature. A schematic overview of the synthesis procedure is also shown in Fig. S1.

2.3. Post-synthetic modification

$Cd(NO_3)_2{\cdot}6H_2O$ (0.4 mmol, 123.4 mg) was dissolved in 3 ml of solvent (methanol or DMF) and 20 mg of ZIF-8 was added into the solution. Then, two different modification strategies were carried out. In one of them, the mixture was placed in a pre-heated oven at 60 °C for 48 h and in the other, the mixture was magnetically stirred at room temperature for 48 h. Each procedure was repeated twice, using methanol or DMF as a solvent. The product obtained for each synthesis was named ZIF-8-A1, ZIF-8-B1, ZIF-8-A2 and ZIF-8-B2, where "A″ or "B″ denotes the solvent used, methanol or DMF respectively, and "1″ or "2" denotes the synthesis conditions, 60 °C or stirring at room temperature respectively. In all cases, the powder was recovered by centrifugation at 6500 rpm and washed three times with fresh methanol. The experimental conditions for the different cation exchange experiments and the corresponding labeling of the obtained samples are summarized in Table S1.

2.4. ZIF-8@PDMS membranes preparation

15 mg of MOF were mixed with a Sylgard® 184 base and a curing agent in a 10:1 wt ratio (1 g and 0.1 g respectively). The mixture was vigorously stirred for 30 min. After the complete dispersion of the MOF powder into the polymer matrix, the mixture was spin-coated on a petri dish at 1000 rpm for 60 s and then placed in an oven at 60 °C overnight. The films were cut and peeled off on demand.

2.5. Sulfide sensing assays

For the sensing experiments, the fluorescence at the maximum emission wavelength of a suspension of ZIF-8 or Cd-doped ZIF-8 (0.5 mg cm^{-3}) was monitored in the absence and presence of different concentrations of Na_2S in aqueous media. To test the sensing capabilities of the ZIF-8@PDMS membranes, 1 × 1 cm of membrane was cut and sticked to a clean quartz substrate and immersed into a sulfide solution in a cuvette compatible with the spectrophotometer with an angle of 45° while the FL changes were monitored. All experiments were carried out at pH 7.4. Note that when Na_2S is dissolved in water, an acid-base equilibrium is

established where SH^- is the specie in higher proportion at the working pH, and the H_2S concentration is negligible [58].

3. Results and discussion

3.1. Characterization

The TEM bright-field and SEM images (Fig. 1) of ZIF-8 crystals reveal that the particles consist of iso-metrical nanoparticles with a narrow size distribution. A statistical evaluation of 100 particles resulted in an average diameter of 56 ± 8 nm. This particle size is consistent with that reported by Cravillon et al. [57].

The MOF material, isolated as a crystalline white powder, was characterized by PXRD (Fig. S2). It is clear that ZIF-8 was obtained as a unique pure phase as the experimental diffraction patter does not show any difference from the simulated one.

The crystallinity of the samples after the cation ex-change was verified by PXRD, as shown in Fig. 2a. Unlike the other post-synthetic modification strategies, the modification conducted to prepare the ZIF-8-A1 sample seems to generate large Zn removal that resulted in the formation of a ZnO phase, observed as a poorly crystallized solid with broad peaks above 30°.

On the other hand, a peak splitting can be observed at 10.5°, plane (200), and 19.5°, plane (400) in the diffractograms of the rest of Cd-doped samples (ZIF-8-A2/B1/B2). Fig. 2b shows a zoom of these two peaks where the splitting can be clearly observed and is attributed to a decrease of the plane symmetry after the incorporation of the Cd atoms. Further analysis shows that the planes (200) and (400) contain the higher density of Zn (II) ions as can be seen in Fig. S3 of the supporting information document, which demonstrates that these planes are more sensitive to small variations of the structure where the metal nodes are involved.

EDS of cation exchanged ZIFs-8 (Fig. S4) exhibits the signals for Cd Lα at 3.12 KeV and for Zn Kα (8.6 KeV), Kβ (9.6 KeV) and Lα (1.01 KeV) indicating the presence of both metals in the MOF structure. As an example, the SEM-EDS mapping of ZIF-8-B1 in Fig. 3 also reveals a homogeneous distribution of Cd^{2+} ions. The amount of cadmium was quantified by WDXRF based on the formula $Zn_{1-x}Cd_x$ (2-Me-Im)$_2$, where x is the metal exchange percentage being 0.8% for ZIF-8-A2, 2.7% for ZIF-8-B1 and 5.1% for ZIF-8- B2. This trend is also observed in the corresponding diffractograms of Fig. 2 where the relative intensity of the split peaks at 10.5° and 19.5° increases with the %Cd in the structure. The incorporation of a bigger atom to a crystal structure involves an increase of the lattice parameters according to Vegard's law [59,60]. Therefore, a bigger unit cell parameter than the pristine ZIF-8 would be expected in the doped samples if the Zn atoms were effectively exchanged by Cd atoms. For this purpose, a Le Bail refinement, as implemented in the FullProf suit of programs [61], was done to ZIF-8 and ZIF-8 doped samples, obtaining an increase of the lat-tice parameter a as the %Cd increases, with values of 17.01 ± 0.04, 17.00 ± 0.01, 17.03 ± 0.03 and 17.23 ± 0.08 Å for pristine ZIF-8, A2, B1 and B2 respectively. The ZIF-8-A1 sample was intentionally excluded from these experiments in order to avoid unrealistic results.

The coordination between the Zn centres and nitrogen atoms of the ligands (2-methylimidazole) was further confirmed by FT-IR, as shown in Fig. S5. As can be seen, both 2Me-HIm and ZIF-8 exhibit the characteristic C=N stretching (1592 cm^{-1}), whereas bands between 1300 and 1500, 1250–900 and 800-600 cm^{-1} can be assigned to the imidazolate ring stretching, in-plane bending and out-of-plane bending respectively [62,63]. The narrow band at

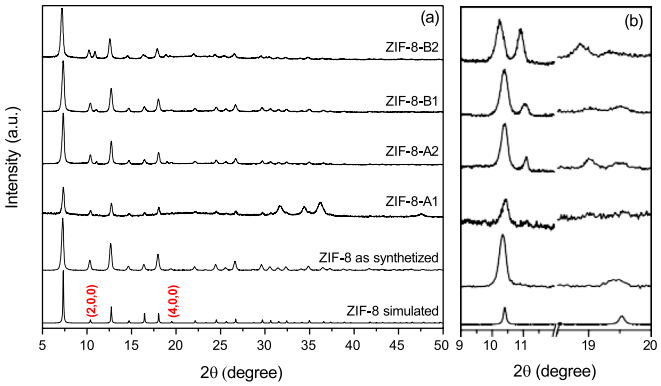

Fig. 2. (a) XRD diffractograms of pristine ZIF-8 and Cd doped ZIFs-8. The planes (200) and (400) are red labelled in their corresponding diffraction peaks. (b) Amplication of the 2θ region of the two peaks of interest.

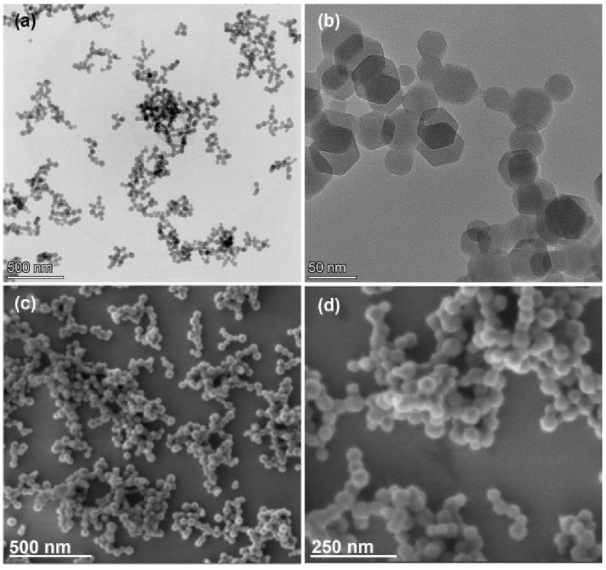

Fig. 1. HR-TEM bright-field images (a–b) and SEM images (c–d) of ZIF-8 nanoparticles with different magnifications.

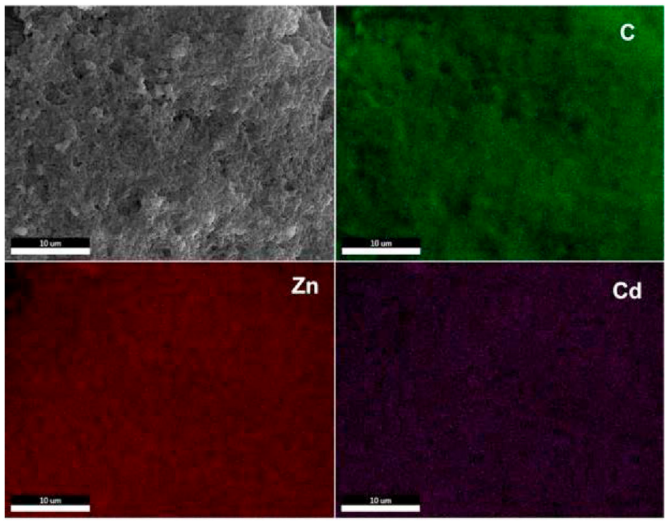

Fig. 3. SEM-EDS mapping of ZIF-8-B1. SEM (top left) and elemental distribution of C Kα (green, top right), Zn Lα (bottom left, red) and Cd Lα (bottom right, purple). The scale bar corresponds to 10 μm.

425 cm^{-1}, attributed to the Zn–N stretching [62,63], and the absence of the typical N–H stretching (3150 cm^{-1}) in the FT-IR spectrum of ZIF-8 indicate the correct coordination between the metal and the ligand. Moreover, the absence of some bands in the spectrum of ZIF-8 compared to that of the free ligand could be explained by the restriction of some vibration modes in the MOF due to the new coordination environ-ment.

The Cd-doped ZIF-8 samples show virtually the same FT-IR spectrum as that of the ZIF-8 (Fig. S6). Be sides, the broad band at 500 cm^{-1} in the FT-IR spectrum of ZIF-8-A1 is assigned to the Zn–O stretching vibration mode of the ZnO [64] formed by the degradation of ZIF-8 during the Cd-doping process. Additionally, the corresponding thermogravimetric analysis (TGA) (Fig. S7) displays a similar profile in all samples except that of the ZIF-8-A1. TGA curves exhibit a slight mass loss (0–4.7%) in the temperature interval of 100–200 °C, attributed to the removal of guest molecules occluded into the MOFs cavities, e.g. DMF or methanol or some species adsorbed on the surface [17]. The subsequent mass loss (55–65%) corresponds to the removal of the ligand, while the remaining mass corresponds to ZnO species. In contrast, the thermogravimetric profile of ZIF-8-A1 shows a minor proportion of ligand-metal, indicating a partial degradation by the formation of ZnO, as shown by the XRD and FT-IR analyses of this sample. In order to avoid interference of this ZnO secondary phase in the sensing properties of the Cd- ZIF-8, the sample ZIF-8-A1 will not be considered in the studies below.

3.2. Luminescent properties

The emission spectra of ZIF-8 and ZIF-8-A2/B1/B2 are shown in Fig. 4. As can be seen, the FL emission intensity of the doped samples is higher in all cases compared with that of the pristine ZIF-8. This enhancement of the FL intensity is notably higher in the ZIF-8-B1 which exhibit a thirty-fold FL emission intensity compared to that of the undoped ZIF-8. It is well known that ZIF-8 displays almost no luminescence and therefore, the FL increase must be unequivocally attributed to the incorporation of the Cd (II) centres, resulting in a Ligand to Metal Charge Transfer (LMCT) between the imidazolate ligands and the Cd^{2+} ions [65]. The inset of Fig. 4 reveals that the light emission increases linearly with the %Cd at least until 2.7%. However, further increase of the Cd content (ZIF-8-B2) does not result in more intense FL, giving rise even to a drastic decrease of the light emission.

In order to understand this phenomenon, the FL excitation spectra of ZIF-8 and ZIF-8-A1/B1/B2 were recorded using the maximum emission wavelength (λ_{em} = 444 nm) as depicted in Fig. 5. As the cadmium content increases, a new band appears in the excitation spectrum with a maximum at 425 nm. This new band is particularly significant in the case of the ZIF- 8-B2 where a clear overlapping with the emission band is observed, producing a reabsorption phenomenon and consequently decreasing the emission efficiency. Therefore, we selected the improved emission properties of the ZIF-8-B1 sample for sensing applications.

3.3. Sulfide ion sensing

Water suspensions (0.5 mg cm^{-3}) of ZIF-8-B1 were exposed to different concentrations of S^{2-} ions *i.e.* 50, 37.5, 25, 5, 2.5, 1.25, 0.5 and 0.05 mM and their emission spectra were recorded at 5, 10 and 15 min of reaction. As shown in Fig. S8a, exposure to increasing concentrations of S^{2-} resulted in a progressive fluorescence quenching of the Cd-doped ZIF-8 material. Specifically, S^{2-} concentrations above 5 mM produced an almost total disappearance of the original emission of the doped MOF. The observed S^{2-} concentration dependence of the response was quantified by using the Stern-Volmer equation (Equation (1))

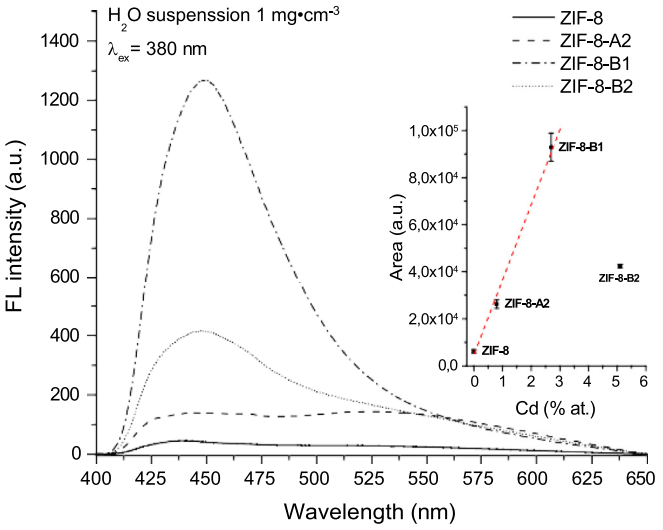

Fig. 4. FL emission spectra of an aqueous suspension (1 mg cm^{-3}) of pristine ZIF-8 (solid line), ZIF-8-A2 (dashed line), ZIF-8- B1 (dashed-dotted line) and ZIF-8-B2 (dotted line). Inset: Area of the FL emission band vs. the Cd atomic content (%). The dashed line represents the expected trend of the FL emission.

$$\frac{A_0}{A} = 1 + K_{SV}\left[S^{2-}\right] \quad (1)$$

where A_0 and A are the area under the FL curves before (A_0) and after (A) S^{2-} exposure, and $K_{S\ V}$ is the Stern-Volmer constant. Fig. S8b shows a perfect fit of the experimental data giving rise to a $K_{S\ V}$ = 828 M^{-1}. From this plot, we can also calculate the limit of

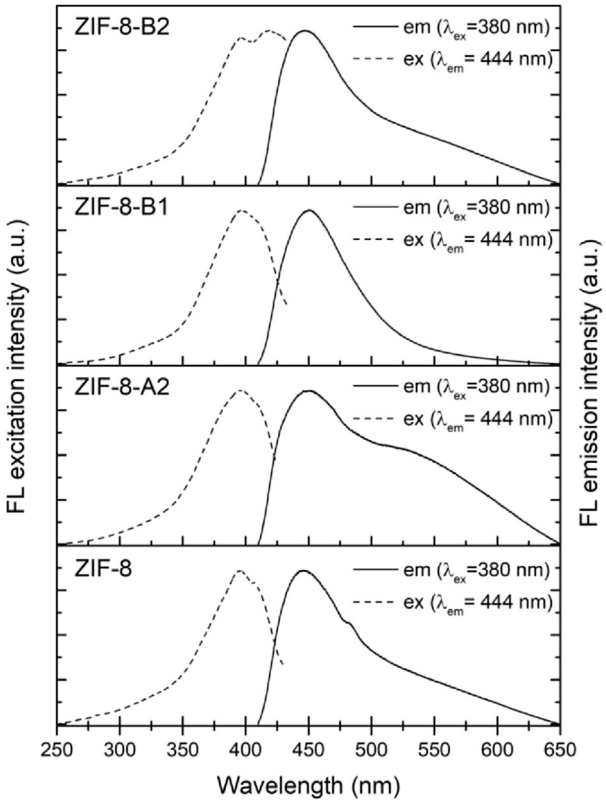

Fig. 5. FL excitation (dashed lines) and emission (solid lines) of a water suspension (0.5 mg cm^{-3}) of pristine ZIF-8, ZIF-8-A2, ZIF-8- B1 and ZIF-8-B2. The corresponding excitation and emission wavelengths are indicated in the figure.

detection (LOD) and the limit of quantification (LOQ) using the linear regression method [66] where $LOD = 3 \times \sigma/slope$ and $LOD = 10 \times \sigma/slope$, with σ standing for the standard deviation of the intercept. The values obtained for the LOD and LOQ were 0.14 and 0.47 mM, respectively. These LOD values are comparable with other found in the literature also using luminescent MOFs for the detection of sulfide ions in solution [67–74]. A table summarizing these results can be found in the supporting information (Table S2).

A time dependence study also reveals a fast decreasing of the FL intensity, reaching the maximum FL changes (quenching) practically 5 min after the exposure to the analyte for all studied concentrations, followed by a stabilization of the curve until a complete saturation is reached (Fig. S9).

In order to understand the sensing mechanism and to test the stability of the sensing material after exposure to the analyte, FT-IR and PXRD measurements were carried out with exposed ZIF-8-B1 powders. As can be seen in the corresponding FT-IR spectrum (Fig. S10a), a new band appears in the 750-450 cm^{-1} region that is attributed to the stretching mode of Cd–S bond, revealing covalent interactions between sulfide ions and the cadmium centres [75,76]. This reaction interrupts the LMCT and subsequently produces a FL quenching. This fact is supported by the presence of the typical N–H stretching band of secondary amines at 3360 cm^{-1} [77]. These results can be understood considering the extremely high tendency toward the formation of CdS ($K_{ps} \approx 10^{-27}$) [78,79], being energetically favorable the breaking of the Cd–N coordination to form CdS. The XRD diffractogram (Fig. S10b) also reveals that the MOF is still crystalline after the analyte exposure. Due to these strong covalent interactions, the recovery of the system was not possible after washing the particles several times with fresh water or methanol (data not shown). Other recovery strategies are in progress and deserve further research.

In order to take advantage of the sensing properties of the ZIF-8-B1 material, a solid sensor was fabricated by its incorporation into a PDMS matrix. The corresponding SEM images (Fig. S11) reveal that the MOF nanocrystallites are totally embedded into the porous polymeric film with a homogeneous thickness of 59 μm. The crystallinity of the MOF, once embedded in the PDMS membrane, was confirmed by μ-XRD (Fig. S12). As can be observed, the diffractogram of ZIF- 8@PDMS reveals that the MOF particles remain crystalline after being incorporated into the PDMS membranes since the main peaks of ZIF-8 can be clearly distinguished from the noisy signal of the mainly amorphous PDMS-based films. Furthermore, the amorphous phase around 12° is attributed to the polymeric matrix.

The FL emission spectrum upon excitation at 380 nm of a ZIF 8-B1@PDMS film is depicted in Fig. 6 along with the corresponding spectrum of an undoped ZIF-8@PDMS film. As expected, the ZIF 8-B1 material embedded in the PDMS films exhibits a similar enhancement of the emission intensity with respect to pure ZIF-8 as compared with the materials suspended in water (Fig. 4a). Moreover, the ZIF 8-B1@PDMS films show the same emission profile as the nanocrystalline MOF material isolated in the form of powder (Fig. S13), and consequently, the membrane exhibits a blue emission, visible with the naked eye, when illuminated under UV light, that is not observed in the corresponding films of pure ZIF-8 (inset in Fig. 6). These results illustrate that the blue emission is due to the presence of the doped ZIF-8 in the membranes.

Exposure of the ZIF-8-B1@PDMS films to low concentrations of Na_2S, *i.e.* 12.5, 1.25 and 0.125 mM, gave rise to a progressive quenching of the film fluorescence until saturation is reached (Fig. S14). More precisely, the kinetic response of the ZIF-8-B1@PDMS membranes was studied by monitoring the temporal evolution of the response (quenching), quantified as $\Phi = 1 - A/A_0$, upon exposure to the same concentration of Na_2S (Fig. 7). The

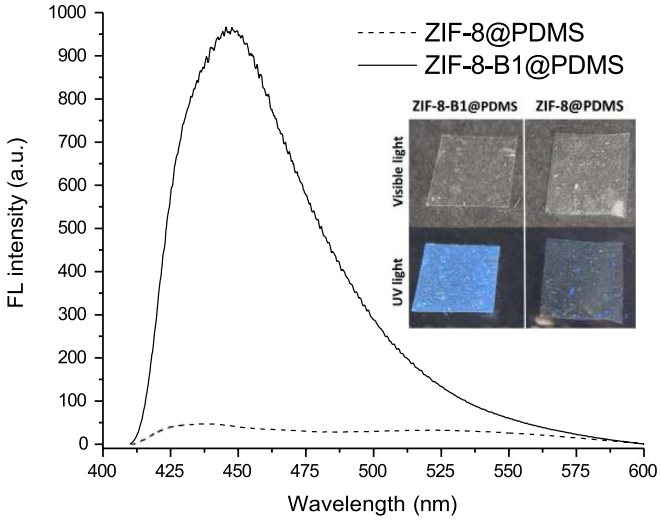

Fig. 6. Fluorescence (λ_{ex} = 380 nm) spectra of ZIF-8@PDMS (dashed line) and ZIF-8-B1@PDMS (solid line) films. Inset: pictures of ZIF-8-B1@PDMS and ZIF-8@PDMS films under visible and UV illumination.

kinetic curves are characterized by a fast response, followed by a stabilization where the complete saturation is easily observed. A numerical fit to these experimental points was carried out by using the two-site Stern-Volmer model [19,20]. Unlike direct exposure of the ZIF-8-B1 suspensions to the analyte, the MOFs particles embedded into the PDMS films can exhibit some degree of heterogeneity and, subsequently, this can involve the presence of two or more sites of interaction, each one with its respective Stern-Volmer constant [80]. The two-site Stern-Volmer equation can be written as a function of Φ as

$$\Phi(t) = 1 - \frac{f_1}{1 + K_1^{SV}\, Q(t)} - \frac{f_2}{1 + K_2^{SV}\, Q(t)} \qquad (2)$$

where f_1 and f_2 are the fraction of each site ($f_1 + f_2 = 1$), K_1^{SV} and K_2^{SV} are their respective Stern-Volmer constants and $Q(t)$ is the quencher uptake at a time *t*. Additionally, it has been demonstrated that diffusion or adsorption-controlled processes are better

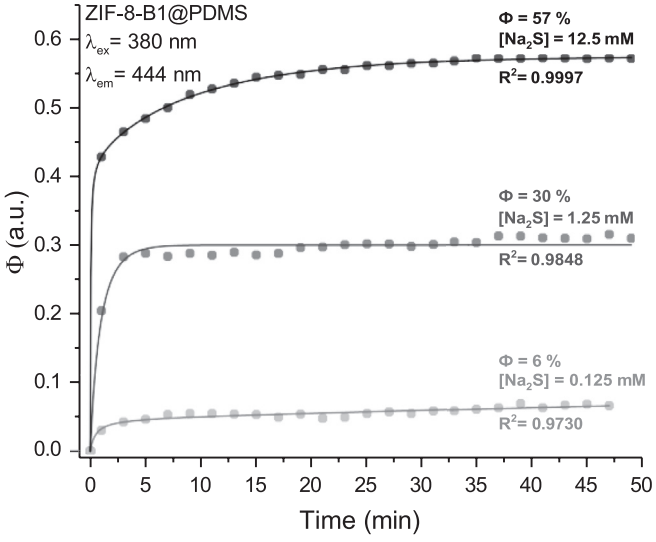

Fig. 7. Kinetic curves obtained (λ_{ex} = 380 nm, λ_{em} = 444 nm) from the exposure of ZIF-8-B1@PDMS films to 12.5, 1.25 and 0.125 mM aqueous solutions of S^{2-}. The dots represent the experimental data and the solid lines the fitted curves.

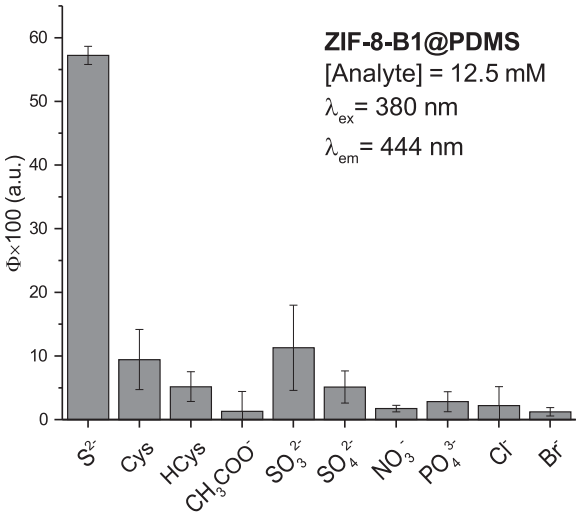

Fig. 8. Response of ZIF-8-B1@PDMS films to common thiols and anions. The error bars represent the standard deviation calculated from three independent measurements.

described by a *pseudo*-second order kinetics [81]. However, diffusion processes where a high uptake is achieved at short times are better described by a *pseudo*-first order kinetics. Hence, $Q(t)$ in Equation (2) is then replaced by the integrated equation of a *pseudo*-first order kinetics (Equation (3)):

$$Q(t) = Q_{\infty}(1 - e^{-kt}) \quad (3)$$

where Q_{∞} is the quencher uptake at equilibrium and k is the kinetic constant. With this approach, a very good agreement with the experimental results was obtained ($R^2 = 0.9997$ for 12.5 mM, $R^2 = 0.9848$ for 1.25 mM and $R^2 = 0.9730$ for 0.125 mM) as can be observed in Fig. 7. Moreover, in order to further analyze the kinetic properties of the material, the t_{50} and t_{90} parameters were calculated from the kinetic curves. These parameters represent the time needed for the sensor to reach 50% and 90% of its maximum response respectively. The t_{50} values were 3.5, 36 and 60 s and the t_{90} values were 520, 156 and 1860 s for 12.5, 1.25 and 0.125 mM respectively. As can be seen, the response times corresponding to the initial part of the response, t_{50}, invariably decrease with the analyte concentration, as expected from a concentration-gradient-driven effect [82]. However, when the response time includes the final part of the response, near the saturation step, t_{90}, relatively high concentrations of the analyte (12.5 mM) lead to a reduction of this value possibly due to a limited diffusion rate in the PDMS membrane. In any case, the obtained values highlight the high response rate in the detection of S^{2-} ions.

Finally, its is important to highlight that the highly specific reaction that takes place during the sensing process ensures the selectivity of the system. As shown in Fig. 8, this selectivity is demonstrated against a set of typical organic and inorganic anions together with organic thiols like cysteine (cys) or homocysteine (Hcys). The FL emission intensity was measured before and after the exposure of ZIF-8-B1@PDMS to 12.5 mM of the possible interferents. In all cases, the quenching obtained is considerably low compared to that obtained in the presence of S^{2-}.

4. Conclusions

The intrinsic fluorescent capacity of ZIF-8 has been increased by a factor of 30 by a post-synthetic doping modification with cadmium, at tetrahedral sites in subsitution of zinc. Secondary light reabsorption appears at higher Cd incorporation, leading to maximum photoemission capacity at 2.7 %Cd content. The photoluminescence of the Cd^{2+} incorporated ZIF-8 is quenched by exposure to sulfide ions in aqueous solution, which has been exploited for sensing application of this ion. The fluorescence quenching follows the Stern-Volmer equation and the sensing is characterized by a fast and sensible response with a LOD of 0.14 mM and a LOQ of 0.47 mM. Cd-ZIF-8 was successfully embedded in polymeric PDMS membranes, retaining excellent sensing capabilities, with t_{50} values in the second range following a pseudo-first order kinetics. Finally, possible interference with other common anions has been studied, demonstrating the selectivity of the material towards sulfide ions. Future work includes the investigation of recovery strategies for the sensor response and its application to the detection of gaseous H_2S.

Author contributions

Francisco G. Moscoso: Writing - Original Draft, Formal analysis **L. Marleny Rodriguez-Albelo:** Methodology, Conceptualization **A. Rabdel Ruiz- Salvador:** Methodology, Conceptualization, Terms **Tânia Lopes-Costa:** Visualization, Supervision **José M. Pedrosa:** Funding acquisition, Project administration, Supervision, Validation.

Declaration of competing interest

The authors declare that they have no known competing financial interests or personal relationships that could have appeared to influence the work reported in this paper.

Data availability

Data will be made available on request.

Acknowledgements

This research has been funded by the Spanish AEI/MCIN/10.13039/501100011033 within the Next Generation EU/PRTR funds through the projects PCI2020-112241 (M-ERA.NET 2019 project 7106, SALMOS) and PID2019-110430 GB-C22 (AD- LIGHT). ERDF (80%) and Andalusian CTEICU/JA in the framework of the Operative Programme FEDER- Andalucia 2014–2020 through projects P20 01258 (objective 01) and UPO-1381028 (objective 1.2.3.) also contributed to the present research. We also thank the laboratory of materials characterization INMALAB of Universidad Pablo de Olavide for experiments and technical support. Funding for open access publishing: Universidad Pablo de Olavide/CBUA.

Appendix A. Supplementary data

Supplementary data to this article can be found online at https://doi.org/10.1016/j.mtchem.2022.101366.

References

[1] H. Furukawa, K.E. Cordova, M. O'Keeffe, O.M. Yaghi, The chemistry and applications of metal-organic frameworks, Science 341 (2013) 1230444–1230444. URL: https://doi.org/10.1126/science.1230444. http://www.ncbi.nlm.nih.gov/pubmed/23990564, http://www.sciencemag.org/cgi/doi/10.1126/science.1230444.

[2] H. Li, M. Eddaoudi, M. O'Keeffe, O.M. Yaghi, Design and synthesis of an exceptionally stable and highly porous metal-organic framework, Nature 402 (1999) 276–279, https://doi.org/10.1038/46248. URL: http://www.nature.com/articles/46248.

[3] W. Lin, W.J. Rieter, K.M.L. Taylor, Modular synthesis of functional nanoscale coordination polymers, Angew. Chem. Int. Ed. 48 (2009) 650–658, https://doi.org/10.1002/anie.200803387.

[4] D. Liu, W. Gu, L. Zhou, L. Wang, J. Zhang, Y. Liu, J. Lei, Recent advances in mof-derived carbon-based nanomaterials for environmental applications in adsorption and catalytic degradation, Chem. Eng. J. 427 (2022) 131503, https://doi.org/10.1016/j.cej.2021.131503.

[5] K. Adil, Y. Belmabkhout, R.S. Pillai, A. Cadiau, P.M. Bhatt, A.H. Assen, G. Maurin, M. Eddaoudi, Gas/vapour separation using ultra-microporous metal–organic frameworks: insights into the structure/separation relationship, Chem. Soc. Rev. 46 (2017) 3402–3430, https://doi.org/10.1039/C7CS00153C. URL: http://xlink.rsc.org/?DOI=C7CS00153C.

[6] T. Rodenas, I. Luz, G. Prieto, B. Seoane, H. Miro, A. Corma, F. Kapteijn, F.X. Llabr=s i Xamena, J. Gascon, Metal–organic framework nanosheets in polymer composite materials for gas separation, Nat. Mater. 14 (2015) 48–55, https://doi.org/10.1038/nmat4113. URL: http://www.nature.com/articles/nmat4113.

[7] Y. Ye, S. Xian, H. Cui, K. Tan, L. Gong, B. Liang, T. Pham, H. Pandey, R. Krishna, P.C. Lan, K.A. Forrest, B. Space, T. Thonhauser, J. Li, S. Ma, Metal–organic framework based hydrogen-bonding nanotrap for efficient acetylene storage and separation, J. Am. Chem. Soc. 144 (2022) 1681–1689, https://doi.org/10.1021/jacs.1c10620.

[8] T. Rajkumar, D. Kukkar, K.-H. Kim, J.R. Sohn, A. Deep, Cyclodextrin-metal–organic framework (CD-MOF): from synthesis to applications, J. Ind. Eng. Chem. 72 (2019) 50–66, https://doi.org/10.1016/J.JIEC.2018.12.048. URL: https://www.sciencedirect.com/science/article/pii/S1226086X1831390X.

[9] S. Mallakpour, E. Nikkhoo, C.M. Hussain, Application of MOF materials as drug delivery systems for cancer therapy and dermal treatment, Coord. Chem. Rev. 451 (2022) 214262, https://doi.org/10.1016/j.ccr.2021.214262.

[10] M. Yoon, R. Srirambalaji, K. Kim, Homochiral metal–organic frameworks for asymmetric heterogeneous catalysis, Chem. Rev. 112 (2012) 1196–1231, https://doi.org/10.1021/cr2003147. URL: http://www.ncbi.nlm.nih.gov/pubmed/22084838 http://pubs.acs.org/doi/10.1021/cr2003147.

[11] A. Corma, H. García, F.X. Llabrés i Xamena, Engineering metal organic frameworks for heterogeneous catalysis, Chem. Rev. 110 (2010) 4606–4655, https://doi.org/10.1021/cr9003924. URL: http://www.ncbi.nlm.nih.gov/pubmed/20359232 http://pubs.acs.org/doi/abs/10.1021/cr9003924.

[12] T. Zhang, W. Lin, Metal-organic frameworks for artificial photosynthesis and photocatalysis, Chem. Soc. Rev. 43 (2014) 5982–5993, https://doi.org/10.1039/c4cs00103f. URL: http://www.ncbi.nlm.nih.gov/pubmed/24769551.

[13] E. Vijayakumar, S. Ramakrishnan, C. Sathiskumar, D.J. Yoo, J. Balamurugan, H.S. Noh, D. Kwon, Y.H. Kim, H. Lee, MOF-derived cop-nitrogen-doped carbon@nifep nanoflakes as an efficient and durable electrocatalyst with multiple catalytically active sites for oer, her, orr and rechargeable zinc-air batteries, Chem. Eng. J. 428 (2022) 131115, https://doi.org/10.1016/j.cej.2021.131115.

[14] Y. Zhou, R. Abazari, J. Chen, M. Tahir, A. Kumar, R.R. Ikreedeegh, E. Rani, H. Singh, A.M. Kirillov, Bimetallic metal–organic frameworks and mof-derived composites: recent progress on electro- and photoelectrocatalytic applications, Coord. Chem. Rev. 451 (2022) 214264, https://doi.org/10.1016/j.ccr.2021.214264.

[15] H. He, Q.-Q. Zhu, Y. Yan, H.-W. Zhang, Z.-Y. Han, H. Sun, J. Chen, C.-P. Li, Z. Zhang, M. Du, Metal–organic framework supported au nanoparticles with organosilicone coating for high-efficiency electrocatalytic n2 reduction to nh3, Appl. Catal. B Environ. 302 (2022) 120840, https://doi.org/10.1016/j.apcatb.2021.120840.

[16] W.P. Lustig, S. Mukherjee, N.D. Rudd, A.V. Desai, J. Li, S.K. Ghosh, Metal–organic frameworks: functional luminescent and photonic materials for sensing applications, Chem. Soc. Rev. 46 (2017) 3242–3285, https://doi.org/10.1039/C6CS00930A. URL: http://xlink.rsc.org/?DOI=C6CS00930A.

[17] J. Roales, F.G. Moscoso, F. Gámez, T. Lopes-Costa, A. Sousaraei, S. Casado, J.R. Castro-Smirnov, J. Cabanillas-Gonzalez, J. Almeida, C. Queirós, L. Cunha-Silva, A.M. Silva, J.M. Pedrosa, Preparation of luminescent metal-organic framework films by soft-imprinting for 2,4-dinitrotoluene sensing, Materials 10 (2017) 992, https://doi.org/10.3390/ma10090992. URL: http://www.ncbi.nlm.nih.gov/pubmed/28841183 http://www.pubmedcentral.nih.gov/articlerender.fcgi?artid=PMC5615647 http://www.mdpi.com/1996-1944/10/9/992.

[18] L.E. Kreno, K. Leong, O.K. Farha, M. Allendorf, R.P. Van Duyne, J.T. Hupp, Metal–organic framework materials as chemical sensors, Chem. Rev. 112 (2012) 1105–1125, https://doi.org/10.1021/cr200324t. URL: http://www.ncbi.nlm.nih.gov/pubmed/22070233http://pubs.acs.org/doi/10.1021/cr200324t.

[19] F.G. Moscoso, J. Almeida, A. Sousaraei, T. Lopes-Costa, A.M.G. Silva, J. Cabanillas-Gonzalez, L. Cunha-Silva, J.M. Pedrosa, A lanthanide MOF immobilized in PMMA transparent films as a selective fluorescence sensor for nitroaromatic explosive vapours, J. Mater. Chem. C 8 (2020) 3626–3630, https://doi.org/10.1039/D0TC00376J. URL: http://xlink.rsc.org/?DOI=D0TC00376J.

[20] F.G. Moscoso, J. Almeida, A. Sousaraei, T. Lopes-Costa, A.M.G. Silva, J. Cabanillas-Gonzalez, L. Cunha-Silva, J.M. Pedrosa, Luminescent MOF crystals embedded in PMMA/PDMS transparent films as effective NO_2 gas sensors, Mol. Syst. Des. Eng. 5 (2020) 1048–1056, https://doi.org/10.1039/C9ME00164F. URL: http://xlink.rsc.org/?DOI=C9ME00164F.

[21] L. Fan, D. Zhao, B. Li, F. Wang, Y. Deng, Y. Peng, X. Wang, X. Zhang, Luminescent binuclear zinc(ii) organic framework as bifunctional water-stable chemosensor for efficient detection of antibiotics and Cr(VI) anions in water, Spectrochim. Acta Mol. Biomol. Spectrosc. 264 (2022) 120232, https://doi.org/10.1016/j.saa.2021.120232.

[22] H. Xu, F. Zhong, F. Chen, T.-X. Luan, P. Li, S. Xu, J. Gao, A Zr-MOF nanoflower sensor and its mixed-matrix membrane for the highly sensitive detection of nitroaromatics, J. Mater. Chem. C 10 (2022) 7469–7475, https://doi.org/10.1039/D2TC00920J.

[23] C. Liu, Y. Bai, W. Li, F. Yang, G. Zhang, H. Pang, In situ growth of three-dimensional mxene/metal–organic framework composites for high-performance supercapacitors, Angew. Chem. Int. Ed. 61 (2022), https://doi.org/10.1002/anie.202116282.

[24] P. Geng, L. Wang, M. Du, Y. Bai, W. Li, Y. Liu, S. Chen, P. Braunstein, Q. Xu, H. Pang, Mil-96-al for Li-S batteries: shape or size? Adv. Mater. 34 (2022) 2107836, https://doi.org/10.1002/adma.202107836.

[25] S. Zheng, Y. Sun, H. Xue, P. Braunstein, W. Huang, H. Pang, Dual-ligand and hard-soft-acid-base strategies to optimize metal-organic framework nanocrystals for stable electrochemical cycling performance, Natl. Sci. Rev. 9 (2022), https://doi.org/10.1093/nsr/nwab197.

[26] J.D. Evans, C.J. Sumby, C.J. Doonan, Post-synthetic metalation of metal-organic frameworks, Chem. Soc. Rev. 43 (2014) 5933–5951, https://doi.org/10.1039/c4cs00076e.

[27] C.K. Brozek, M. Dinca, Cation exchange at the secondary building units of metal–organic frameworks, Chem. Soc. Rev. 43 (2014) 5456–5467, https://doi.org/10.1039/C4CS00002A. URL: http://xlink.rsc.org/?DOI=C4CS00002A.

[28] K.S. Park, Z. Ni, A.P. Côté, J.Y. Choi, R. Huang, F.J. Uribe-Romo, H.K. Chae, M. O'Keeffe, O.M. Yaghi, Exceptional chemical and thermal stability of zeolitic imidazolate frameworks, Proc. Natl. Acad. Sci. 103 (2006) 10186–10191, https://doi.org/10.1073/pnas.0602439103. URL: https://pnas.org/doi/full/10.1073/pnas.0602439103.

[29] D.W. Lewis, A.R. Ruiz-Salvador, A. Gómez, L.M. Rodriguez-Albelo, F.-X. Coudert, B. Slater, A.K. Cheetham, C. Mellot-Draznieks, Zeolitic imidazole frameworks: structural and energetics trends compared with their zeolite analogues, CrystEngComm 11 (2009) 2272, https://doi.org/10.1039/b912997a. URL: http://xlink.rsc.org/?DOI=b912997a.

[30] Y. Hwang, A. Phan, K. Galatsis, O.M. Yaghi, R.N. Candler, Zeolitic imidazolate framework-coupled resonators for enhanced gas detection, J. Micromech. Microeng. 23 (2013), https://doi.org/10.1088/0960-1317/23/12/125027.

[31] H. Tian, H. Fan, M. Li, L. Ma, Zeolitic imidazolate framework coated ZnO nanorods as molecular sieving to improve selectivity of formaldehyde gas sensor, ACS Sens. 1 (2016) 243–250, https://doi.org/10.1021/acssensors.5b00236. URL: https://pubs.acs.org/doi/10.1021/acssensors.5b00236.

[32] A.I. Khudiar, A.K. Elttayef, M.K. Khalaf, A.M. Oufi, Fabrication of gas sensors for selective gas detection, Mater. Res. Express 6 (2020) 126450, https://doi.org/10.1088/2053-1591/ ab69c2. URL: ZnO@ZIF-8 https://iopscience.iop.org/article/10.1088/2053-1591/ab69c2.

[33] P.G. Choi, Z. Liu, N. Hara, Y. Masuda, Surface molecular separator for selective gas sensing, Ind. Eng. Chem. Res. 59 (2020) 17894–17900, https://doi.org/10.1021/acs.iecr.0c03395. URL: https://pubs.acs.org/doi/10.1021/acs.iecr.0c03395.

[34] S.S. Nair, N. Illyaskutty, B. Tam, A.O. Yazaydin, K. Emmerich, A. Steudel, T. Hashem, L. Schöttner, C. Wöll, H. Kohler, H. Gliemann, ZnO@ZIF-8: gas sensitive core-shell hetero-structures show reduced cross-sensitivity to humidity, Sensor. Actuator. B Chem. 304 (2020) 127184, https://doi.org/10.1016/j.snb.2019.127184. URL: https://linkinghub.elsevier.com/retrieve/pii/S0925400519313838.

[35] L. Tian, Y. Sun, H. Huang, X. Guo, Z. Qiao, J. Meng, C. Zhong, Porous ZIF-8 thin layer coating on ZnO hollow nanofibers for enhanced acetone sensing, ChemistrySelect 5 (2020) 2401–2407, https://doi.org/10.1002/slct.201904137. URL: https://onlinelibrary.wiley.com/doi/10.1002/slct.201904137.

[36] H. Karimi-Maleh, R. Darabi, M. Shabani-Nooshabadi, M. Baghayeri, F. Karimi, J. Rouhi, M. Alizadeh, O. Karaman, Y. Vasseghian, C. Karaman, Determination of d & c red 33 and patent blue v azo dyes using an impressive electrochemical sensor based on carbon paste electrode modified with zif-8/g-c3n4/co and ionic liquid in mouthwash and toothpaste as real samples, Food Chem. Toxicol. 162 (2022) 112907, https://doi.org/10.1016/j.fct.2022.112907.

[37] M. Zhan, C. Ge, S. Hussain, A.S. Alkorbi, R. Alsaiari, N.A. Alhemiary, G. Qiao, G. Liu, Enhanced NO_2 gas-sensing performance by core-shell sno2/zif-8 nanospheres, Chemosphere 291 (2022) 132842, https://doi.org/10.1016/j.chemosphere.2021.132842.

[38] Q. Zhou, L. Xu, Z. Kan, L. Yang, Z. Chang, B. Dong, X. Bai, G. Lu, H. Song, A multi-platform sensor for selective and sensitive H_2S monitoring: three-dimensional macroporous zno encapsulated by mofs with small pt nanoparticles, J. Hazard. Mater. 426 (2022) 128075, https://doi.org/10.1016/j.jhazmat.2021.128075.

[39] J. Fu, S. Zhou, P. Zhao, X. Wu, S. Tang, S. Chen, Z. Yang, Z. Zhang, A dual-response ratiometric fluorescence imprinted sensor based on metal-organic frameworks for ultrasensitive visual detection of 4-nitrophenol in environments, Biosens. Bioelectron. 198 (2022) 113848, https://doi.org/10.1016/j.bios.2021.113848.

[40] L. Zhang, Y. Xu, J. Xu, H. Zhang, T. Zhao, L. Jia, Intelligent multicolor nanosensor based on nontoxic dual fluoroprobe and mofs for colorful consecutive detection of Hg^{2+} and cysteine, J. Hazard. Mater. 430 (2022) 128478, https://doi.org/10.1016/j.jhazmat.2022.128478.

[41] Y. Song, D. Hu, F. Liu, S. Chen, L. Wang, Fabrication of fluorescent SiO_2@zeolitic imidazolate framework-8 nanosensor for Cu^{2+} detection, Analyst 140 (2015) 623–629, https://doi.org/10.1039/C4AN01773K. URL: http://xlink.rsc.org/?DOI=C4AN01773K.

[42] Y. Xia, Y. Hong, R. Geng, X. Li, A. Qu, Z. Zhou, Z. Zhang, Amine-functionalized ZIF-8 as a fluorescent probe for breath volatile organic compound biomarker detection of lung cancer patients, ACS Omega 5 (2020) 3478–3486, https://doi.org/10.1021/acsomega.9b03793. URL: https://pubs.acs.org/doi/10.1021/acsomega.9b03793.

[43] Y. Wang, B. Wang, H. Shi, C. Zhang, C. Tao, J. Li, Carbon nanodots in ZIF-8: synthesis, tunable luminescence and temperature sensing, Inorg. Chem. Front. 5 (2018) 2739–2745, https://doi.org/10.1039/C8QI00637G. URL: http://xlink.rsc.org/?DOI=C8QI00637G.

[44] T.-T. Han, J. Yang, Y.-Y. Liu, J.-F. Ma, Rhodamine 6G loaded zeolitic imidazolate framework-8 (ZIF-8) nanocomposites for highly selective luminescent sensing of Fe^{3+} Cr^{6+} and aniline, Microporous Mesoporous Mater. 228 (2016) 275–288, https://doi.org/10.1016/j.micromeso.2016.04.005. URL: https://linkinghub.elsevier.com/retrieve/pii/S1387181116300853.

[45] H. Guo, X. Wang, N. Wu, M. Xu, M. Wang, L. Zhang, W. Yang, One-pot synthesis of a carbon dots@zeolitic imidazolate framework-8 composite for enhanced Cu^{2+} sensing, Anal. Methods 12 (2020) 4058–4063, https://doi.org/10.1039/D0AY01121E. URL: http://xlink.rsc.org/?DOI=D0AY01121E.

[46] X. Lin, G. Gao, L. Zheng, Y. Chi, G. Chen, Encapsulation of strongly fluorescent carbon quantum dots in metal–organic frameworks for enhancing chemical sensing, Anal. Chem. 86 (2014) 1223–1228, https://doi.org/10.1021/ac403536a. URL: https://pubs.acs.org/doi/10.1021/ac403536a.

[47] Y.-B. Hao, Z.-S. Shao, C. Cheng, X.-Y. Xie, J. Zhang, W.-J. Song, H.-S. Wang, Regulating fluorescent aptamer-sensing behavior of zeolitic imidazolate framework (ZIF-8) platform via lanthanide ion doping, ACS Appl. Mater. Interfaces 11 (2019) 31755–31762, https://doi.org/10.1021/acsami.9b12253. URL: https://pubs.acs.org/doi/10.1021/acsami.9b12253.

[48] J. Gao, C. Wang, H. Tan, Dual-emissive polystyrene@zeolitic imidazolate framework-8 composite for ratiometric detection of singlet oxygen, J. Mater. Chem. B 5 (2017) 9175–9182, https://doi.org/10.1039/C7TB02684F.

[49] Y. Ling, L.Z. He, C.C. Wan, L. Han, X.H. Wang, Z.Y. Xu, X.L. Li, N.B. Li, H.Q. Luo, ZIF-8@gmp-tb nanocomplex for ratiometric fluorescent detection of alkaline phosphatase activity, Spectrochim. Acta Mol. Biomol. Spectrosc. 264 (2022) 120230, https://doi.org/10.1016/j.saa.2021.120230.

[50] S. Liu, Z. Xiang, Z. Hu, X. Zheng, D. Cao, Zeolitic imidazolate framework-8 as a luminescent material for the sensing of metal ions and small molecules, J. Mater. Chem. 21 (2011) 6649, https://doi.org/10.1039/c1jm10166h. URL: http://xlink.rsc.org/?DOI=c1jm10166h.

[51] A.P. Vargas, F. Gámez, J. Roales, T. Lopes-Costa, J.M. Pedrosa, A paper-based ultrasensitive optical sensor for the selective detection of H2S vapors, Chemosensors 9 (2021) 40, https://doi.org/10.3390/chemosensors9020040.

[52] Y. Bhambhani, M. Singh, Physiological effects of hydrogen sulfide inhalation during exercise in healthy men, J. Appl. Physiol. 71 (1991) 1872–1877, https://doi.org/10.1152/jappl.1991.71.5.1872.

[53] R.O. Beauchamp, J.S. Bus, J.A. Popp, C.J. Boreiko, D.A. Andjelkovich, P. Leber, A critical review of the literature on hydrogen sulfide toxicity, CRC Crit. Rev. Toxicol. 13 (1984) 25–97, https://doi.org/10.3109/10408448409029321.

[54] S. He, B. Zhu, X. Jiang, G. Han, S. Li, C.H. Lau, Y. Wu, Y. Zhang, L. Shao, Symbiosis-inspired de novo synthesis of ultrahigh MOF growth mixed matrix membranes for sustainable carbon capture, Proc. Natl. Acad. Sci. 119 (2022), https://doi.org/10.1073/pnas.2114964119.

[55] B.B. Mohammed, H. Lgaz, A.A. Alrashdi, K. Yamni, N. Tijani, Y. Dehmani, H.E. Hamdani, I.-M. Chung, Insights into methyl orange adsorption behavior on a cadmium zeolitic-imidazolate framework Cd-ZIF-8: a joint experimental and theoretical study, Arab. J. Chem. 14 (2021) 102897, https://doi.org/10.1016/j.arabjc.2020.11.003.

[56] J. Sun, L. Semenchenko, W.T. Lim, M.F.B. Rivas, V. Varela-Guerrero, H.-K. Jeong, Facile synthesis of cd-substituted zeolitic-imidazolate framework Cd-ZIF-8 and mixed-metal CdZn-ZIF-8, Microporous Mesoporous Mater. 264 (2018) 35–42, https://doi.org/10.1016/j.micromeso.2017.12.032.

[57] J. Cravillon, S. Müncer, S.-J. Lohmeier, A. Feldhoff, K. Huber, M. Wiebcke, Rapid room-temperature synthesis and characterization of nanocrystals of a prototypical zeolitic imidazolate framework, Chem. Mater. 21 (2009) 1410–1412, https://doi.org/10.1021/cm900166h. URL: https://pubs.acs.org/doi/10.1021/cm900166h.

[58] M. House, W.J. Weiss, Review of microbially induced corrosion and comments on needs related to testing procedures, Purdue University Libraries Scholarly Publishing Services, 2014, pp. 94–103, https://doi.org/10.5703/1288284315388.

[59] K.T. Jacob, S. Raj, L. Rannesh, Vegard's law: a fundamental relation or an approximation? Int. J. Mater. Res. 98 (2007) 776–779, https://doi.org/10.3139/146.101545. URL: https://www.degruyter.com/document/doi/10.3139/146.101545/html.

[60] M. Magomedov, On the deviation from the Vegard's law for the solid solutions, Solid State Commun. 322 (2020) 114060, https://doi.org/10.1016/j.ssc.2020.114060. URL: https://linkinghub.elsevier.com/retrieve/pii/S0038109820305639.

[61] R.E. Dinnebier, S.J.L. Billinge (Eds.), Powder Diffraction, Royal Society of Chemistry, Cambridge, 2008, https://doi.org/10.1039/9781847558237. URL: http://ebook.rsc.org/?DOI=10.1039/9781847558237.

[62] M. Adnan, K. Li, L. Xu, Y. Yan, X-shaped ZIF-8 for immobilization rhizomucor miehei lipase via encapsulation and its application toward biodiesel production, Catalysts 8 (2018) 96, https://doi.org/10.3390/catal8030096. URL: http://www.mdpi.com/2073-4344/8/3/96.

[63] Y. Hu, H. Kazemian, S. Rohani, Y. Huang, Y. Song, In situ high pressure study of ZIF-8 by FTIR spectroscopy, Chem. Commun. 47 (2011) 12694, https://doi.org/10.1039/c1cc15525c. URL: http://xlink.rsc.org/?DOI=c1cc15525c.

[64] R. Zamiri, A. Rebelo, G. Zamiri, A. Adnani, A. Kuashal, M.S. Belsley, J.M.F. Ferreira, Far-infrared optical constants of ZnO and ZnO/Ag nanostructures, RSC Adv. 4 (2014) 20902–20908, https://doi.org/10.1039/C4RA01563K. URL: http://xlink.rsc.org/?DOI=C4RA01563K.

[65] Y.-Q. Tian, L. Xu, C.-X. Cai, J.-C. Wei, Y.-Z. Li, X.-Z. You, Determination of the solvothermal synthesis mechanism of metal imidazolates by X-ray single-crystal studies of a photoluminescent cadmium(II) imidazolate and its intermediate involving piperazine, Eur. J. Inorg. Chem. 2004 (2004) 1039–1044, https://doi.org/10.1002/ejic.200300560. URL: http://doi.wiley.com/10.1002/ejic.200300560.

[66] M.M. Sanagi, S.L. Ling, Z. Nasir, D. Hermawan, W.A. Wan Ibrahim, A.A. Naim, Comparison of signal-to-noise, blank determination, and linear regression methods for the estimation of detection and quantification limits for volatile organic compounds by gas chromatography, J. AOAC Int. 92 (2009) 1833–1838, https://doi.org/10.1093/jaoac/92.6.1833. URL: https://academic.oup.com/jaoac/article/92/6/1833-1838/5655972.

[67] S.S. Nagarkar, T. Saha, A.V. Desai, P. Talukdar, S.K. Ghosh, Metal-organic framework based highly selective fluorescence turn-on probe for hydrogen sulphide, Sci. Rep. 4 (2015) 7053, https://doi.org/10.1038/srep07053.

[68] S.S. Nagarkar, A.V. Desai, S.K. Ghosh, A nitro-functionalized metal-organic framework as a reaction-based fluorescence turn-on probe for rapid and selective H_2S detection, Chem. Eur. J. 21 (2015) 9994–9997, https://doi.org/10.1002/chem.201501043.

[69] S. Nandi, H. Reinsch, S. Banesh, N. Stock, V. Trivedi, S. Biswas, Rapid and highly sensitive detection of extracellular and intracellular H_2S by an azide-functionalized Al(III)-based metal–organic framework, Dalton Trans. 46 (2017) 12856–12864, https://doi.org/10.1039/C7DT02293J.

[70] X. Zhang, J. Zhang, Q. Hu, Y. Cui, Y. Yang, G. Qian, Postsynthetic modification of metal–organic framework for hydrogen sulfide detection, Appl. Surf. Sci. 355 (2015) 814–819, https://doi.org/10.1016/j.apsusc.2015.07.166.

[71] A. Buragohain, S. Biswas, Cerium-based azide- and nitro-functionalized uio-66 frameworks as turn-on fluorescent probes for the sensing of hydrogen sulphide, CrystEngComm 18 (2016) 4374–4381, https://doi.org/10.1039/C6CE00032K.

[72] R. Song, L. Hou, Y. Wang, Y. Li, X. Wang, Y. Zang, Y. Zang, X. Wang, S. Yan, Fluorescence Zn-based metal–organic frameworks for the detection of hydrogen sulfide in natural gas, Anal. Methods 9 (2017) 3914–3919, https://doi.org/10.1039/C7AY01193H.

[73] X. Zhang, Q. Zhang, D. Yue, J. Zhang, J. Wang, B. Li, Y. Yang, Y. Cui, G. Qian, Flexible metal-organic framework-based mixed-matrix membranes: a new platform for H_2S sensors, Small 1801563 (2018) 1801563, https://doi.org/10.1002/smll.201801563. URL: http://doi.wiley.com/10.1002/smll.201801563.

[74] X. Zhang, Q. Hu, T. Xia, J. Zhang, Y. Yang, Y. Cui, B. Chen, G. Qian, Turn-on and ratiometric luminescent sensing of hydrogen sulfide based on metal–organic frameworks, ACS Appl. Mater. Interfaces 8 (2016) 32259–32265, https://doi.org/10.1021/acsami.6b12118.

[75] S.R.K. Pandian, V. Deepak, K. Kalishwaralal, S. Gurunathan, Biologically synthesized fluorescent CdS NPs encapsulated by PHB, Enzym. Microb. Technol. 48 (2011) 319–325, https://doi.org/10.1016/j.enzmictec.2011.01.005. URL: https://linkinghub.elsevier.com/retrieve/pii/S0141022911000238.

[76] N. Susha, K. Nandakumar, S.S. Nair, Enhanced photoconductivity in CdS/betanin composite nanostructures, RSC Adv. 8 (2018) 11330–11337, https://doi.org/10.1039/C7RA13116J. URL: http://xlink.rsc.org/?DOI=C7RA13116J.

[77] B.H. Stuart, Infrared Spectroscopy: Fundamentals and Applications, Analytical Techniques in the Sciences, John Wiley & Sons, Ltd, Chichester, UK, 2004, https://doi.org/10.1002/0470011149. URL: http://doi.wiley.com/10.1002/0470011149.

[78] T.F. Towey, A. Khan-Lodhi, B.H. Robinson, Kinetics and mechanism of formation of quantum-sized cadmium sulphide particles in water–aerosol-ot–oil microemulsions, J. Chem. Soc. Faraday Trans. 86 (1990) 3757–3762, https://doi.org/10.1039/FT9908603757.

[79] P.C. Rieke, S.B. Bentjen, Deposition of cadmium sulfide films by decomposition of thiourea in basic solutions, Chem Mater 5 (1993) 43–53, https://doi.org/10.1021/cm00025a012.

[80] J.N. Demas, B.A. DeGraff, W. Xu, Modeling of luminescence quenching-based sensors: comparison of multisite and nonlinear gas solubility models, Anal. Chem. 67 (1995) 1377–1380, https://doi.org/10.1021/ac00104a012. URL: https://pubs.acs.org/doi/abs/10.1021/ac00104a012.

[81] J.-P. Simonin, On the comparison of pseudo-first order and pseudo-second order rate laws in the modeling of adsorption kinetics, Chem. Eng. J. 300 (2016) 254–263, https://doi.org/10.1016/j.cej.2016.04.079. URL: https://linkinghub.elsevier.com/retrieve/pii/S1385894716305290.

[82] D.J. Rankin, L. Bocquet, D.M. Huang, Entrance effects in concentration-gradient-driven flow through an ultrathin porous membrane, J. Chem. Phys. 151 (2019) 044705, https://doi.org/10.1063/1.5108700.